THE ASTROPHYSICAL JOURNAL, 485:859–868, 1997 August 20

COLLISIONLESS RECONNECTION AND HIGH-ENERGY PARTICLE ACCELERATION IN SOLAR FLARES

BORIS V. SOMOV[1] AND TAKEO KOSUGI
National Astronomical Observatory of Japan, Mitaka, Tokyo 181, Japan
Received 1996 October 22; accepted 1997 March 25

ABSTRACT

Observations with the Hard X-Ray Telescope (HXT) and the Soft X-Ray Telescope (SXT) on board *Yohkoh* show that the reconnection process is common to impulsive and gradual flares. We apply the collisionless reconnection theory—more exactly, the model of a high-temperature turbulent-current sheet (HTTCS)—to the coronal conditions derived from the *Yohkoh* data on the site and mechanism of magnetic energy transformation into kinetic and thermal energies of "superhot" plasma and accelerated particles. We consider the reconnecting current sheet as the source of flare energy and the first-step mechanism in a two-step acceleration of electrons and ions to high energies.

According to our model, reconnected field lines rapidly move out of the HTTCS, being frozen into superhot plasma, and form magnetic loops on the upstream side of a fast oblique collisionless shock (FOCS) situated above the soft X-ray–emitting loops of a strong magnetic field. The electrons and ions energized and preaccelerated by the HTTCS are trapped in magnetic loops. The top of each loop moves with a high speed toward the FOCS, while its feet penetrate through the shock front. For these reasons, two mechanisms—the adiabatic heating inside the collapsing trap and acceleration by the shock front at the two feet of the trap—efficiently increase the particle energy.

The lifetime of an individual collapsing trap can be identified with the observed few-second delay to higher energies of hard X-ray and gamma-ray emission. The trap of accelerated electrons can be seen as the coronal hard X-ray "above-the-loop-top source." Precipitation of accelerated electrons from the trap through the FOCS into the chromosphere is responsible for the hard X-ray "footpoint sources." The model explains timing, location, and motion of the hard X-ray sources in solar flares as well as the observed relative intensity of the coronal and chromospheric hard X-ray sources and other physical properties.

Subject headings: acceleration of particles — MHD — Sun: flares — Sun: particle emission — Sun: X-rays, gamma rays

1. INTRODUCTION

Magnetic reconnection plays a key role in the dynamics of astrophysical plasmas, especially in solar flares (Giovanelli 1946; Hones 1984). Reconnection serves as a highly efficient engine to convert magnetic energy into thermal and kinetic energies of plasma flows and accelerated particles (e.g., Somov 1994). However, before *Yohkoh*, there was little clear evidence that reconnection is responsible for the primary release of flare energy. Solar hard and soft X-ray observations (Kosugi et al. 1991; Tsuneta et al. 1991) on board *Yohkoh* suggest that reconnection is responsible for many nonsteady phenomena in the corona. In particular, in many flares the reconnection of magnetic field lines takes place. Reconnection seems to be common to impulsive (compact) and gradual (large-scale) flares.

In this paper, we consider the collisionless reconnecting current sheet (RCS) as the source of flare energy as well as the first-step mechanism of particle acceleration. In § 2 we introduce the model of high-temperature turbulent-current sheets (HTTCS) under coronal conditions observed by *Yohkoh*. The acceleration of electrons and ions in the HTTCS is briefly discussed in § 2.5 as a preacceleration mechanism. Section 3 deals with the magnetic trap created by reconnected field lines between the HTTCS and the FOCS. Because the length of this trap rapidly decreases from a large initial scale to zero, we call it a "collapsing trap." In § 4 we discuss the possible contribution of the FOCS to particle acceleration inside the collapsing trap. The features of X-ray emission explained by our model are presented in § 5. Comparison of our model with other models is given in § 6. At the end, in § 7, we formulate our conclusions.

[1] On leave from Astronomical Institute, Moscow State University, Moscow 119899, Russia.

2. HTTCS AS A FLARE ENERGY SOURCE

2.1. *Simplest Current-Sheet Model*

Let us recall two approximations used to study reconnection in current sheets. The first is the *neutral*-sheet model (e.g., Sweet 1969; Syrovatskii 1981). This was initially the simplest two-dimensional MHD model of steady reconnection. Two oppositely directed magnetic fields are pushed together into the neutral sheet. The uniform field $\boldsymbol{B}_0$ outside the sheet is frozen into the uniform plasma inflow with velocity $\boldsymbol{v}_0$ perpendicular to the field. The plasma flows out of the sheet through its edges with large velocity $\boldsymbol{v}_1$ perpendicular to the velocity $\boldsymbol{v}_0$. By definition, there is no magnetic field inside the sheet; that is why it is called neutral. Although it is an idealization, the neutral-sheet model is still useful for several reasons.

First, this model demonstrates the existence of two linear scales corresponding to two different physical processes: (*a*) The dissipative thickness $2a \approx 2v_m v_0^{-1}$ is responsible for the reconnection rate; here v_m is the magnetic diffusivity. (*b*) The sheet width $2b$ is responsible for the accumulation of magnetic energy; the wider the neutral sheet, the larger the energy accumulated.

Second, the neutral-sheet model permits very efficient acceleration of particles in the RCS (Speiser 1965).

Let us take as the low limits for the field $B_0 \approx 50$ G and for the velocity $v_0 \approx 20$ km s^{-1}. These values are smaller than those estimated from the *Yokhoh* observations of the well-studied flare on 1992 January 13—the magnetic field 52 G and the inflow speed 41–143 km s^{-1} (Tsuneta et al. 1997).

So the lower limit for the electric field is

$$E_0 = \frac{1}{c} v_0 B_0 \approx 1 \text{ V cm}^{-1} . \quad (1)$$

This field is much stronger than Dreicer's field,

$$E_{cr} = \frac{4\pi e^3}{k_B} (\ln \Lambda) \frac{n}{T} \approx 10^{-4} \text{ V cm}^{-1} . \quad (2)$$

Here we have assumed that the density and temperature of the plasma near the RCS are respectively $n_0 \approx 4 \times 10^8$ cm^{-3} and $T_0 \approx 3 \times 10^6$ K. In fact, near the RCS in flares, the magnetic field B_0 can be as high as 100–300 G. So the electric field E_0 can be even stronger by 1 order of magnitude.

Since $E_0 \gg E_{cr}$, we can neglect collisional energy losses as well as wave-particle interaction of fast particles (e.g., Gurevich & Zhivlyuk 1966). Thus the neutral-sheet model predicts very impulsive acceleration by the strong electric field $\boldsymbol{E}_0$. This important advantage is discussed in § 2.5, taking account of the fact that real reconnecting sheets are always nonneutral, i.e., they always have an internal magnetic field. The influence of this three-component field on particle acceleration is a key point in § 2.5.

2.2. *Magnetically Nonneutral RCS*

Neutrality of the RCS, as assumed above, means that there is no penetration of field lines through the sheet (the transverse field $\boldsymbol{B}_\perp = 0$) as well as no magnetic field parallel to the electric current inside the RCS (the longitudinal field $\boldsymbol{B}_\parallel = 0$). In general, both assumptions are incorrect (for a review see Somov 1992; Longcope & Cowley 1996).The first of these is the most important for what follows.

As it reconnects, every field line penetrates through the RCS (Fig. 1). Thus the reconnecting sheet is magnetically nonneutral by definition, because of the physical meaning of reconnection. In many real cases (for example, the magnetospheric tail or interplanetary current sheets) a small transverse magnetic field is always observed. This is also the case of laboratory and numerical experiments (Hesse et al. 1996; Ono et al. 1996; Horiuchi & Sato 1997).

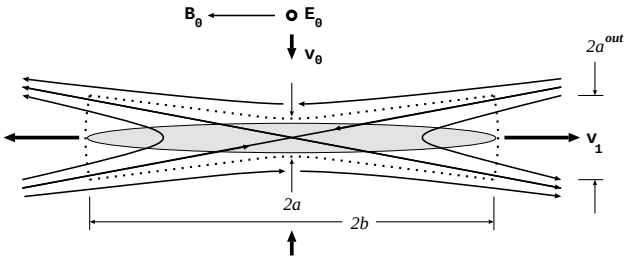

FIG. 1.—Three characteristic scales of the nonneutral sheet: $2a$ is a dissipative thickness, the electric current distribution is shown by shading, $2b$ is a scale responsible for energy accumulation, and the dotted boundary indicates the field lines going through the sheet, so $2a^{out}$ is the scale which determines the outflow of energy and mass.

We characterize the penetration of magnetic field into the sheet by the parameter $\xi_\perp = B_\perp/B_0$. As distinguished from the neutral sheet, we assume that

$$a/b \ll \xi_\perp \ll 1 . \quad (3)$$

The penetration of even a very small field component into the high-temperature sheet essentially increases the outflows of energy and mass along the magnetic field lines. The effective cross section for the outflows is proportional to the scale

$$a^{out} \approx \xi_\perp b \gg a . \quad (4)$$

Even a very small ($\xi_\perp \approx 10^{-3}$) transverse field $\boldsymbol{B}_\perp$ significantly increases the conductive cooling of the nonneutral HTTCS. As a result, its energy output is much larger than that of the neutral one. (In the neutral sheet $a^{out} = a$.) The last reason enables us to consider the HTTCS with a small transverse magnetic field as the source of flare energy.

2.3. *Basic Physics of the HTTCS*

Coulomb collisions do not play any role in the HTTCS. Thus the plasma inside the HTTCS has to be considered as essentially collisionless. The concept of an anomalous resistivity, which originates from wave-particle interactions, is then useful to describe the fast conversion from field energy to particle energy. Some general properties of such collisionless reconnection can be examined in the frame of a self-consistent model based on the mass, momentum, and energy conservation laws.

A particular feature of this model is that electrons and ions are heated by wave-particle interactions in a different way; contributions to the energy balance are not made by the energy exchange between electrons and ions due to collisions, or by the thermal flux across the magnetic field, or by the energy losses for radiation. The magnetic field–aligned thermal flux becomes anomalous and plays the dominant role in the cooling of the electrons in the HTTCS. These properties are typical for collisionless plasma in solar flares and can be taken into account by two equations describing the balance of energy for electrons and ions separately:

$$\chi_{ef} \mathscr{E}^{in}_{mag} = \mathscr{E}^{out}_{t,e} + \mathscr{C}^{an}_{\parallel} , \quad (5)$$

$$(1 - \chi_{ef}) \mathscr{E}^{in}_{mag} = \mathscr{E}^{out}_{t,i} + \mathscr{K}^{out}_{i} . \quad (6)$$

Here χ_{ef} is a relative fraction of the heating consumed by electrons from the magnetic enthalpy flux $\mathscr{E}_{mag}$, while the remaining fraction $(1 - \chi_{ef})$ goes to the ions. The sum of the left-hand sides of equations (5) and (6) represents the direct heating of ions and electrons due to their interactions with waves inside the HTTCS.

In what follows n_s is the plasma density inside the HTTCS; $T = T_e$ is an effective electron temperature (the mean kinetic energy of chaotic motion per single electron), T_i is the effective temperature of ions, and the ratio θ is equal to T_e/T_i. Because of the difference between the effective temperatures of electrons and ions, the electron and ion

enthalpy outflows also differ: $\mathscr{E}_{t,e}^{\rm out} \neq \mathscr{E}_{t,i}^{\rm out}$. The ion kinetic energy flux, $\mathscr{K}_i^{\rm out}$, is important in equation (6). As to the kinetic energy of electrons, it is negligible and is disregarded in equation (5). However, electrons play the dominant role in the anomalous heat conductive cooling $\mathscr{C}_{\|}^{\rm an}$.

In the conditions of flares, the characteristic parameters (for more detail see Somov 1992) of such collisionless current sheets are the following: (*a*) The effective electron temperature T_e is $\approx$100–200 MK; the temperature ratio θ is $\approx$6.5, and the plasma compression n_s/n_0 is $\approx$4.8. (*b*) The dissipative thickness $2a \approx 20$ cm is small, but the width $2b \approx (1\text{–}2) \times 10^9$ cm is large; for this reason the linear scale (eq. [4]) for the outflows of energy and mass $2a^{\rm out} \approx (3\text{–}6) \times 10^6$ cm is not small. (*c*) The energy release power per unit length $\mathscr{L}_j$ (along the direction of the current) is

$$\frac{P_s}{\mathscr{L}_j} = \frac{B_0^2}{4\pi} v_0 4b \approx (1\text{–}7) \times 10^{19} \text{ ergs (s cm)}^{-1} , \qquad (7)$$

if the inflow velocity $v_0 \approx 10\text{–}30$ km s^{-1}. Hence, if the length $\mathscr{L}_j \approx 3 \times 10^9$ cm, then the power of energy release P_s is $\approx 3 \times 10^{28}\text{–}2 \times 10^{29}$ ergs s^{-1}. The outflow velocity is $v_1 \approx 1400\text{–}1800$ km s^{-1}.

2.4. *Fast Plasma Outflows and Shocks*

Fast outflows of superhot collisionless plasma create complicated dynamics in an external (relative to the RCS) region; this dynamics should be a topic of special research. It is clear that the interaction of the fast flow of superhot plasma with external plasma and magnetic field strongly depends on the initial and boundary conditions, especially on the relative position of the outflow source (the HTTCS) and the magnetic "obstacle"—the region of strong external field. Near the boundary of this region the energy of the fast outflow becomes equal to the energy of the external magnetic field that tries to stop the flow.

Let us assume that the distance l_1 between the source of a fast outflow (an edge of the HTTCS) and the stagnation point at the obstacle is not too large (Fig. 2). This means that the fast outflow becomes wider but does not relax in the coronal plasma before reaching the obstacle. Moreover, if the flow velocity still exceeds the local fast magnetoacoustic wave velocity, a fast MHD shock wave appears ahead of the magnetic obstacle, which is similar to the terrestrial bow shock ahead of the magnetosphere.

By analogy with the ordinary hydrodynamics of supersonic flows, we assume that the shock front reproduces the shape of the obstacle smoothly and on a larger scale (Fig. 3); more exactly, it reproduces the shape of the upper part of the obstacle facing the incoming flow. This is true if the incoming flow is uniform or quasi-uniform. Generally speaking, the incoming flow may differ significantly from a quasi-uniform one. In this case, the shock may have a much more complicated shape. This is, however, not of crucial importance for the effect of the collapsing magnetic trap discussed below. The width w_1 of the shock is important. For simplicity, in Figure 3, we assume that all the field lines ejected by the HTTCS penetrate through the shock. This means that all superhot plasma and all particles preaccelerated by the HTTCS, being frozen into the reconnected field lines, interact with the shock. Different complications related to the actual three-dimensional geometry of the magnetic field in an active region occur but will not be discussed in this paper.

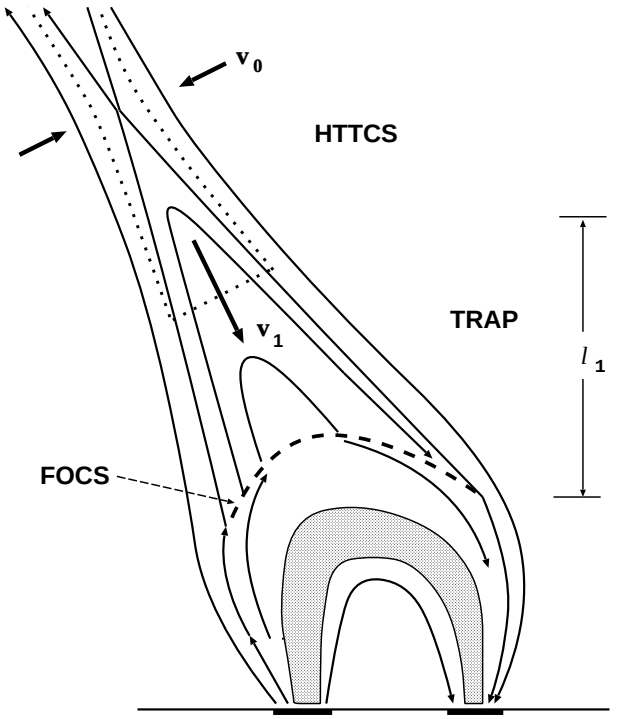

FIG. 2.—HTTCS as a source of flare energy; "superhot" plasma outflow with velocity v_1. The magnetic obstacle is the soft X-ray loop shown by shading.

For what follows, the most important point is that with respect to the particles preaccelerated and to the superhot particles energized by the HTTCS, the shock should be considered as a *fast oblique collisionless* shock (FOCS). Behind the FOCS, the downstreaming plasma becomes more and more collisional. Taking account of its conductive and radiative cooling, the hydrodynamic relaxation of the flow can be stimulated by thermal instability (Field 1965) or by chromospheric "evaporation" driven by accelerated particles precipitating into the chromosphere (see chap. 2 in Somov 1992).

We do not discuss in this paper the possible existence of slow or fast MHD shocks (or other MHD discontinuities) that may be attached to external edges of the collisionless HTTCS. We assume that such discontinuities do not have a direct influence on the collapsing trap effect introduced in § 3.

2.5. *Particle Acceleration in HTTCS*

The acceleration by the electric field $\boldsymbol{E}_0$ and scattering of particles by plasma turbulence in the HTTCS lead to the appearance of electrons with a power-law spectrum and with energies higher than tens of keV (Litvinenko & Somov 1991).

The maximum particle energy can be estimated by taking into account the electric field $\boldsymbol{E}_0$ and three components of the magnetic field $\boldsymbol{B} = \{B_0, B_\perp, B_\|\}$.

The transverse field $\boldsymbol{B}_\perp$ serves to eject an accelerating particle rapidly out of the RCS (Speiser 1965); however, the longitudinal field $\boldsymbol{B}_\|$ tends to counteract this effect (Litvinenko & Somov 1993). The longitudinal component on the order of the reconnecting component B_0 is a necessary condition to accelerate electrons up to 10–100 keV. So

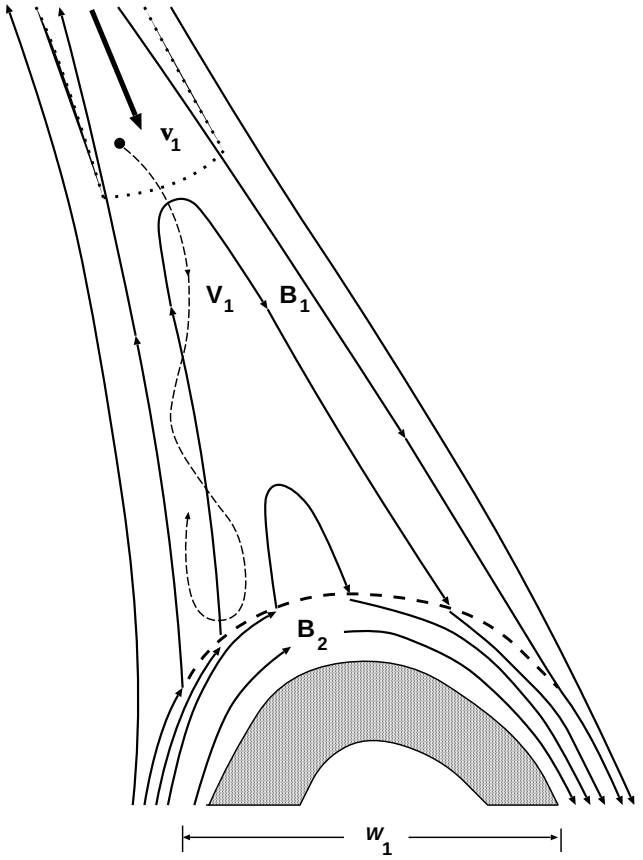

FIG. 3.—Magnetic trap between the HTTCS and the shock front; accelerated particles move with velocity V_1 along the field lines.

we consider the HTTCS as the first-step mechanism in a two-step acceleration of electrons to high energies in flares (for a review see Somov 1994).

For estimates, we shall assume that, on average, the electrons preaccelerated by the HTTCS have an energy $\mathscr{E}_1 \approx 30$ keV or a velocity $V_1 \approx 0.3c$.

In order to understand the ion acceleration, the transverse electric field $\boldsymbol{E}_\perp$ outside the HTTCS must be taken into account. This field is always present as a consequence of charge separation owing to the difference in the electron and proton masses. It appears that the transverse field $\boldsymbol{E}_\perp$, being relatively weak ($e\phi_\perp \approx k_B T$), can, however, efficiently lock ions in the vicinity of the HTTCS, thus allowing their acceleration by a strong electric field $\boldsymbol{E}_0$ (Litvinenko & Somov 1995).

Preaccelerated electrons are frozen into the field lines reconnected by the RCS and moving down (Fig. 3) together with the superhot plasma. Its electron temperature T_e is $\approx$100–200 MK, and the effective temperature of protons T_p is $\approx$15–30 MK. In a field $B_1 \approx 30$ G the electrons with velocity V_1 have initial values of the Larmor radius $r_L^{(e)} \approx 20$ cm; for protons with the same velocity the Larmor radius $r_L^{(p)} \approx 3 \times 10^4$ cm. So preaccelerated protons also can be considered as frozen.

For superhot plasma, the collisional relaxation times can be estimated as follows: The electron collisional time τ_{ee}(200 MK) is $\approx$17 s, the collisional time for protons τ_{pp} is $\approx$ 45 s, and the time for electron-proton collisions, τ_{ep}, is the longest one, $\approx 10^3$ s. Here we assume some average value of the density like $n_1 \approx 2 \times 10^9$ cm^{-3} (Tsuneta et al. 1997; Masuda et al. 1994, 1995) in an extended region of the superhot plasma relaxation. Therefore, to some large extent ($v_1\tau$), the superhot plasma can be considered as colllisionless. For preaccelerated electrons and protons the collisionless approximation is fulfilled much better.

3. COLLAPSING TRAP EFFECT

3.1. *Trap with Shock Wave*

Being frozen into superhot plasma, the reconnected field lines move out of the HTTCS and form magnetic loops at the height l_1 above the magnetic obstacle (Fig. 3). The top of each loop moves with a high velocity $v_1 \approx$ 1400–1800 km s^{-1}. The local fast magnetoacoustic wave speed is $\approx$1000 km s^{-1}. Thus a fast shock may appear between the HTTCS and the magnetic obstacle. Let us assume that both feet of a loop penetrate through the shock front ahead of the obstacle. The opposite assumption is discussed in § 3.2.

Depending on velocity and pitch angle, some of the fast particles preaccelerated by the HTTCS may pass directly through the magnetic field jump related to the shock. Others may either simply be reflected by the shock front or interact with it as discussed in § 4.

For the fast particles reflected by the shock the magnetic loop represents a trap whose length decreases from $\approx 2l_1$ to zero (collapses) with the velocity $\approx 2v_1$. Therefore, the lifetime of each magnetic field line—of each collapsing trap—is equal to

$$t_1 \approx l_1/v_1 \approx 10 \text{ s} , \tag{8}$$

if $l_1 \approx 10^4$ km and $v_1 \approx 10^3$ km s^{-1} are taken as the characteristic values for the length and velocity, respectively.

During the collapsing trap lifetime t_1 the reflected fast particles move between two magnetic "corks"—the reflecting points where the field line crosses the shock front. Since these "corks" move toward each other with the high velocity $2v_1$, the particles trapped inside the trap are "heated" quickly by the first-order Fermi-type mechanism (Fermi 1954).

(Wentzel 1963) considered a MHD shock intersecting one magnetic field line in two points. In such a case the two intersections of the shock with the field line form a single trap ahead of the shock. As the shock moves, the trap becomes shorter, the trapped particles are accelerated, and the number of accelerations per second increases. The collapsing trap effect discussed in our paper is the equivalent situation, which may be classified as a variant of the Wentzel trap.

For the fast electrons and ions preaccelerated by the HTTCS we estimated the characteristic value of velocity as $V_1 \approx 10^{10}$ cm s^{-1}. Hence the characteristic time between two subsequent reflections of a particle can be estimated as

$$\tau_1 \approx 2l_1/V_1 \approx 0.2 \text{ s} . \tag{9}$$

Since $\tau_1 \ll t_1$, the conditions of periodic longitudinal motions slowly change *adiabatically*. Then the *longitudinal* adiabatic invariant is conserved:

$$I = \oint p_\parallel \, dl \approx p_\parallel(t) 4l(t) = \text{constant} . \tag{10}$$

Here $p_\parallel = p \cos \Theta$ is the particle longitudinal momentum, and Θ is its pitch angle.

From equation (10) it follows that

$$p_{\parallel}(t) = p_{\parallel}(0)\,\frac{l_1}{l(t)} \approx p_{\parallel}(0)\,\frac{1}{1-(t/t_1)}\,. \tag{11}$$

When the trap collapses, the longitudinal momentum grows infinitely within the time t_1. Neglecting an unknown change of the transverse momentum, we see that the particle energy increases within the timescale t_1:

$$\mathscr{E} = \frac{p^2}{2m} = \mathscr{E}(0)\,\frac{1}{[1-(t/t_1)]^2}\,. \tag{12}$$

That is why we can assume that just trap lifetime t_1 can be responsible for an observed few-second delay in higher energies of hard X-ray and gamma-ray emission (Bai et al. 1983). We assume that the few-second bursts observed in hard X-ray emission can be related to the collapsing trap effect. The consequences of this assumption are discussed in § 5.

The main objection usually raised against Fermi acceleration is that the Fermi mechanism is "neither efficient nor selective." A magnetic mirror reflects particles on a nonselective basis: thermal particles may be reflected as well as suprathermal ones. Hence, most of the primary energy—the kinetic energy of the fast flow of superhot plasma—goes into bulk heating of the plasma rather than the selective acceleration of only a small minority of fast particles. This "disadvantage" appears to be the main *advantage* of the Fermi mechanism when applied to solar flares in the frame of our model.

First, the collapsing trap heats and compresses the superhot plasma. Thus it becomes more visible in hard X-ray emission. This possibility will be discussed in § 5.1. Second, the same Fermi mechanism can lift some electrons from a quasi-thermal distribution and accelerate them to higher energies; even better, it can further accelerate the electrons preaccelerated by the HTTCS. The trap of accelerated electrons can be seen as the nonthermal component of the coronal hard X-ray source in flares (§ 5.2). Third, being nonselective, the collapsing trap can accelerate not only electrons but also protons and other ions to high energies. This is a big problem for other acceleration mechanisms.

3.2. *Trap without Shock*

If, contrary to the assumption made above, the distance l_1 between the HTTCS and the stagnation point is large enough, then the fast flow of superhot plasma relaxes gradually with (or without) collisional shock depending on the height of the reconnection site and other conditions in an active region where the flare occurs (e.g., Tsuneta 1996). For example, collisional relaxation can be very fast near the HTTCS if the plasma density is relatively high but the temperature inside the current sheet is relatively low.

Let us consider the configuration of a magnetic trap with field lines rapidly moving down but without any shock (Fig. 4). In this case, instead of equation (11) we have

$$p_{\parallel}(t) \approx p_{\parallel}(0)\,\frac{l_1 + l_2}{l_2 + (l_1 - v_1\,t)}$$

$$\Rightarrow p_{\parallel}(0)\,\frac{l_1 + l_2}{l_2} \quad \text{when} \quad t \to t_1\,. \tag{13}$$

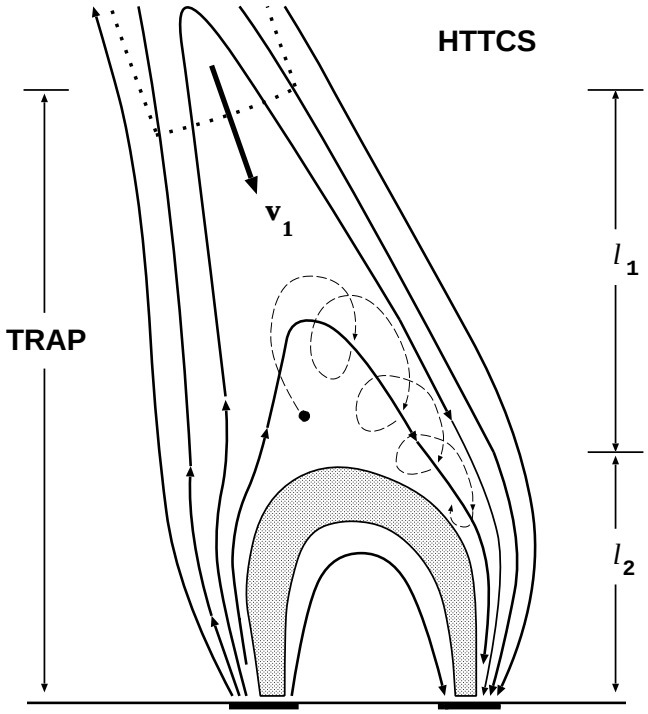

FIG. 4.—Magnetic trap without a shock

So the trap does not collapse. If the height l_2 of the magnetic obstacle is not small, the adiabatic heating of fast particles inside the trap is less efficient than in the collapsing trap with the shock. The small height l_2 is probably the case of the so-called shrinkage of X-ray loops, as observed by the *Yohkoh* SXT in the active region AR 7240 in 1993 February (Wang et al. 1997).

4. ACCELERATION BY SHOCK WAVE

4.1. *Diffusive Mechanism*

The interaction of fast particles with the FOCS should be considered quantitatively in several aspects: reflection and passage (in terms of our model, trapping and precipitation of particles from the trap into the chromosphere), and acceleration (an additional energization of the trapped particles over their adiabatic heating). Analytical models of particle acceleration by shocks (see Jones & Ellison 1991; Blandford 1994) illustrate the possible high efficiency of diffusive and drift accelerations to high energies.

In diffusive acceleration, the particle energies are derived just from the relative motion (the converging flow) between "scatterers" (waves) on either side of a shock front. This is a major advantage of the diffusive mechanism. Its disadvantage in applying to our model consists of a lack of knowledge about these assumed scattering waves. Many assumptions that are not well justified have to be made concerning the shock-associated turbulence.

4.2. *Drift Acceleration*

The drift mechanism, in contrast to the diffusive one, neglects any shock-associated turbulence. If the Larmor radius r_L (see § 2.5) of the fast particle is much larger than the front thickness, one can replace the shock by a simple

discontinuity and approximate the particle motion as scatter-free on both sides of the shock.

Since we consider the shock front as a discontinuity, the adiabatic approximation is formally not suitable. If, however, the *transversal* invariant is conserved (see the very clear physical justification in the classical paper by Wentzel 1963),

$$\frac{p_\perp^2}{B} = \text{constant} , \tag{14}$$

then

$$p_{\perp 2}^2 = p_{\perp 1}^2 \left(\frac{B_2}{B_1} \right) . \tag{15}$$

Here B_1 and B_2 are the upstream and downstream values of the magnetic field (see Fig. 3). Hence, the transverse kinetic energy of a nonrelativistic particle is

$$\frac{\mathscr{E}_{\perp 2}}{\mathscr{E}_{\perp 1}} = \frac{p_{\perp 2}^2}{p_{\perp 1}^2} \propto \frac{B_2}{B_1} . \tag{16}$$

In this way, adiabatic theory predicts an increase of particle energy by a fast ($B_2 > B_1$) oblique shock but a decrease of energy by a slow ($B_2 < B_1$) shock.

Note that the adiabatic "heating" of fast particles in the collapsing trap mainly increases the longitudinal energy, while the drift acceleration gives rise to the transverse energy. By so doing, the drift acceleration improves the trapping conditions for accelerating particles.

The increase of transverse energy (eq. [16]) is relatively small when the Larmor orbit of a particle crosses the front only once (see Toptyghin 1980). Multiple interactions of a particle with the shock is a necessary condition for a considerable increase of energy. Our model, which is a combination of the FOCS with the trap returning the reflected particles to the shock, seems to be optimal in this sense.

A similar situation in which the particles are trapped and accelerated on the upstream side of a collisionless shock is found in the example of drift acceleration at interplanetary shocks (Gisler & Lemons 1990; Balogh & Erdos 1991; Erdos & Balogh 1994). The collapse of the trap by its convection through the shock is accompanied by a considerable increase of the accelerated particle flux.

4.3. *Quantitative Analysis*

A quantitative model of these phenomena is desirable but not simple. Two-dimensional hybrid simulations (Thomas & Winske 1990) of a curved collisionless shock (like the bow shock) have shown that (*a*) the fast ions originate on the quasi-parallel upstream side of the shock and (*b*) energization of the ions is just drift acceleration that requires multiple shock encounters. This behavior of ions is qualitatively similar to what we assumed above, but quantitative comparison of the simulation results with our model is difficult because of the large difference in physical conditions.

Time-reversed numerical integration of trajectories has been performed by Erdos & Balogh (1994) to study the particles trapped upstream of an interplanetary shock. It is shown that the effectiveness of the acceleration is enhanced by multiple interactions with the shock. This is an important factor at higher energies where the smaller energy gain at each reflection by a shock might be partly compensated by a greater number of shock encounters.

5. X-RAY EMISSION SIGNATURE

5.1. *Hard X-Ray "Above-the-Loop-Top Source"*

To explain the hard X-ray and gamma-ray time profiles in several flares, first-order Fermi-type acceleration of particles between two shocks moving toward each other inside a closed loop was suggested by Bai et al. (1983) as a mechanism for the second-step acceleration of prompt protons and relativistic electrons. It was assumed that fast electrons penetrate into the flare loop and rapidly heat the upper chromosphere to high temperatures (Lin & Hudson 1976; Somov & Spektor 1982). As a consequence of chromospheric "evaporation," shocks move upward from both footpoints. Fast particles are reflected only by colliding with the shock fronts.

Bai et al. (1983) assumed that an unknown first-step mechanism accelerates protons and electrons above the "injection energy," at which the collisional energy loss equals the energy gain due to the Fermi process. Our model suggests that the first step is the acceleration of electrons and ions by the HTTCS, and the second step is the fast adiabatic heating and acceleration by a collisionless shock located *above* the flare loop discussed by Bai et al. (1983). So we assume (after Kosugi 1996) that trapped accelerated electrons create the coronal hard X-ray "above-the-loop-top source" observed by the *Yohkoh* HXT (Masuda et al. 1994, 1995).

An alternative possibility was discussed by Wheatland & Melrose (1995). High-density ($\approx 10^{12}$ cm^{-3}) regions are assumed and presumably observed (Feldman et al. 1994) at the tops of the soft X-ray–emitting loops. Electrons "accelerated by the flare" encounter the dense small regions creating "intermediate thick-thin target" hard X-ray emission. If we could arbitrarily introduce an ambient density high enough to explain the hard X-ray intensity of the above-the-loop-top source, the trap considered in our model would not be required. This is not the case, however; the ambient density determined from *Yohkoh* SXT observations is much lower (Kosugi 1996).

It is not clear in the model by Wheatland & Melrose (1995) whether the displacement between the soft X-ray loop top and the hard X-ray above-the-loop-top source (Masuda et al. 1994, 1995) has been considered (Aschwanden et al. 1996a).

Superhot plasma trapped inside the collapsing loops certainly can also contribute to the hard X-ray and radio emission above the soft X-ray–emitting loop (Gopalswamy et al. 1995; Sakao & Kosugi 1996). The total coronal hard X-ray emission consists of two parts: nonthermal and quasi-thermal. Our model predicts, however, a significant difference between them. Being more collisional, the superhot plasma is less confined inside the trap. For this reason the nonthermal emission dominates at higher energies and occupies a more compact "vertical" (Fig. 5) hard X-ray source in comparison with more extended "horizontal" distribution of a quasi-thermal emission at lower energies. This seems to be consistent with recent results by Tsuneta et al. (1997).

Heat transfer in the superhot plasma certainly differs from the collisional diffusive conduction. "Quasi-thermal" electrons escape from the trap and generate a strong reverse electric current. The electric field driving this reverse current efficiently limits the heat transfer by "quasi-thermal" electrons (Diakonov & Somov 1988). Excitation of ion-acoustic

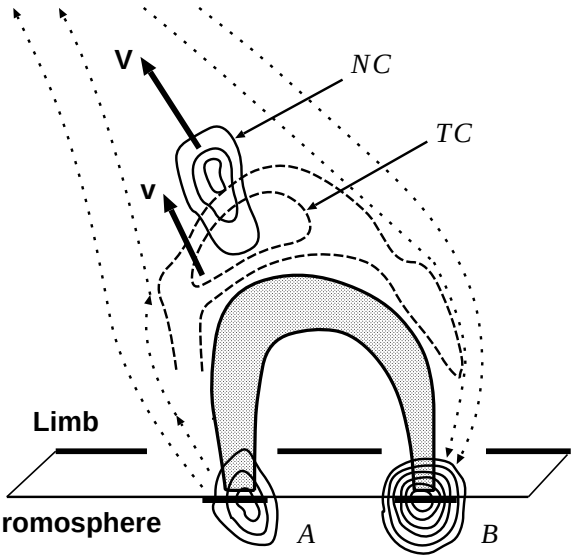

FIG. 5.—Sketch of nonthermal (NC) and quasi-thermal (TC) components of the coronal hard X-ray emission and their apparent motion. A and B are the chromospheric "footpoint sources."

waves by the reverse current can determine the speed of the "quasi-thermal" front propagation. This does not contradict the observed expansion speed of the coronal hard X-ray source (Takakura et al. 1993).

5.2. *Hard X-Ray "Footpoint Sources"*

According to our model, precipitation of accelerated electrons from the trap through the fast oblique collisionless shock into the chromosphere is responsible for the hard X-ray "footpoint sources." This scenario is consistent with the electron time-of-flight analysis for Masuda's flare of 1992 January 13 (Aschwanden et al. 1996b; for statistical studies see Aschwanden et al. 1996d, 1996c).

In five flares, observed simultaneously with BATSE on board *CGRO* and the HXT on board *Yohkoh*, coronal hard X-ray sources of the Masuda type in the cusp region have been found. The electron time-of-flight analysis provides independent evidence that particle acceleration in these flares occurs in the cusp region above the flare loop and that the coronal hard X-ray sources are a signature of this acceleration site (Aschwanden et al. 1996c).

According to Kosugi (1996), the intensity ratio of the above-the-loop-top source to footpoint sources suggests that fast electrons mirror and make cyclical bounce motions inside a trap over the integrated column thickness

$$\zeta_{\rm tr} = n_1 V_1 t_{\rm tr} \ {\rm cm}^{-2} \tag{17}$$

of the order of one-tenth of the column thickness,

$$\zeta_{\rm max} = \frac{\mathscr{E}^2}{2a_1} \ {\rm cm}^{-2} , \tag{18}$$

that they pass before completely losing their kinetic energy $\mathscr{E}$ measured in keV. Here $a_1 = 1.3 \times 10^{-19}[\ln(\mathscr{E}/mc^2) - (\ln n)/2 + 38.7]$ keV^2 cm^2. For electrons with an initial energy $\mathscr{E}_{\rm in} \approx 100$ keV we have $a_1 \approx 3.4 \times 10^{-18}$ keV^2 cm^2.

So, on the one hand, we estimate the maximal column thickness $\zeta_{\rm max} \approx 1.5 \times 10^{21}$ cm^{-2}, which corresponds to the 100 keV electrons that precipitate from the trap through the FOCS into the thick target—the chromosphere—where they are stopped. On the other hand, since these electrons have the initial velocity $V_1 \approx 1.2 \times 10^{10}$ cm s^{-1}, we can estimate the minimal time the electrons must be trapped to produce the observed relative brightness of the coronal and chromospheric hard X-ray sources:

$$t_{\rm tr} \approx r\left(\frac{\zeta_{\rm max}}{n_1 V_1}\right) \approx 6 \ {\rm s} . \tag{19}$$

Here $r \approx 0.1$ is the observed intensity ratio, and $n_1 \approx 2 \times 10^9$ cm^{-3}, as in § 3.

Therefore, the fast electrons with the initial energy $\mathscr{E}_{\rm in} \approx 100$ keV must have at least $t_{\rm tr}/\tau_1 \approx 30$ reflections inside the trap. If they make this number of reflections, the trapping time (eq. [19]) is still shorter than the lifetime of the collapsing loop (eq. [8]).

Note that τ_1 is defined as the travel time (between two consecutive reflections) at the beginning of the trap collapsing process, when the length of the trap is maximal. Toward the end of the collapsing at $t \approx t_1$, much more frequent reflections occur. This effect is obviously not small. In addition, in the simple estimate (eq. [19]), we have neglected an increase of electron energy, which also increases the frequency of reflections and which is not small either. Both effects, neglected in equation (19), increase the efficiency of particle acceleration by the collapsing trap.

Let us substitute the trapping time (eq. [19]) into equation (12). We find that electrons with initial energy $\mathscr{E}_{\rm in} \approx 100$ keV can be accelerated by the first-order Fermi-type mechanism to an energy $\mathscr{E}_{\rm max} \approx 600$ keV; the higher the initial energy of the electrons preaccelerated by the HTTCS, the higher the efficiency of acceleration in the collapsing trap.

For electrons with lower energy—for example, $\mathscr{E}_{\rm in} = \mathscr{E}_1 \approx 30$ keV—the minimal trapping time is much shorter: $t_{\rm tr} \approx 0.7$ s. Comparing this time with equation (9), we see that several reflections of the 30 keV electrons from the FOCS are enough to explain the observed ratio of hard X-rays coming from the thin-target above-the-loop-top source and from the thick-target footpoint sources. However, substitution of $t_{\rm tr} \approx 0.7$ s in equation (12) gives $\mathscr{E}_{\rm max} \approx 35$ keV. This means that, even in the early beginning of the collapsing process, when the adiabatic heating of the 30 keV electrons is still very slow, it can overcome the energy loss processes in the trap. That is why the collapsing trap is a potential mechanism for lifting electrons out of a very low energy distribution, as assumed above, or even out of a thermal population (see test particle simulations by Gisler & Lemons 1990). At later stages of the collapsing process, the adiabatic heating becomes more and more efficient.

The estimated times from equation (19) do not contradict the following fact. Although the above-the-loop-top source is weak in comparison with the double footpoint sources by about an order of magnitude (which is taken into account in eq. [19]), it varies its intensity similarly but smoothly (see § 5.5) to the footpoint sources, i.e., impulsively, as far as the effective temporal resolution of several to 10 seconds is concerned (Kosugi 1996; Aschwanden et al. 1996b).

5.3. *Acceleration or Heating?*

Very effective heating but inefficient acceleration seems to be typical for the type A (hot thermal) flares (Tanaka 1987;

Dennis 1988). These flares have the following set of hard X-ray characteristics: (1) Temporal (gradual rise and fall at energies below ≈ 40 keV, weak impulsive emission at higher energies). (2) Spectral (thermal fit below 40 keV with temperatures of $3–4 \times 10^7$ K; very steep spectra above 40 keV with power-law index $\gamma \geq 7$). (3) Spatial (compact size [less than 6000 km] and low height [less than 6000 km]).

On the contrary, the type C (gradual hard) flares appear to be very efficient accelerators. They have (1) gradually varying hard X-ray emission; (2) spectrum above ≈ 50 keV hardening with time, with γ decreasing monotonically from ≥ 5 early in the flare to ≤ 2 later in the flare after the peak; and (3) high altitudes of $\geq 4 \times 10^4$ km. So, in type C flares, continuous particle acceleration may occur at high altitudes, where the density and magnetic field must be much lower than for the low-altitude type A and type B (ordinary impulsive) flares. In type A flares, the energy release appears to result primarily in heating to temperatures of $(3–4) \times 10^7$ K with little acceleration. According to Tanaka (1987) and Dennis (1988), this is possibly because of a higher density at the energy release site.

According to our model, the primary energy source—the HTTCS—can provide high-temperature (say 30–40 MK) plasma and low-energy (≈ 30 keV for electrons) particles in all three types of flares. As for higher energies, we assume that the second-step acceleration mechanism is necessary, and it can be the first-order Fermi-type acceleration in the collapsing magnetic trap. In § 3.2 we saw that the trap does not collapse if there is no shock between the HTTCS and the magnetic obstacle—the soft X-ray loop. In this section we point out that the collapsing trap effect is sensitive to the plasma density.

If the density is not as low as assumed in § 2.5 ($n_1 \approx 2 \times 10^9$ cm^{-3}), then with increase of density the Coulomb collisions become important. They scatter electrons into the loss cone. This is the so-called weak diffusion process, which neglects possible wave-particle interactions responsible for strong diffusion. Anyway, diffusion of electrons into the loss cone increases precipitation of them from the trap. So the collapsing trap acceleration will not work if plasma density inside the trap is high enough. This seems to be the case for very compact flares in the upper chromosphere or low corona.

According to Aschwanden et al. (1996a), for 78 flares, observed with *Yohkoh* and *CGRO* simultaneously, electron trapping is governed by weak diffusion, while scattering by waves seems to be unimportant. A mean value of electron density in the trap is $\approx 10^{11}$ cm^{-3}, which is as high as in the soft X-ray brightest loops. Hence, for a majority of flares (presumably type B) analyzed by Aschwanden et al. (1996a), the second-step acceleration might be not as efficient as collisional heating. On the contrary, the type C flares are certainly the class of flares where the collapsing trap acceleration can work efficiently because of much lower plasma density inside the trap.

5.4. *Soft X-Ray Emission*

In the double footpoint sources, the precipitating fast particles impulsively heat the upper chromosphere to temperatures $T_{ev} \approx 10^7$ K. In general, the hydrodynamic and radiative response of the chromosphere to impulsive heating by beams of accelerated particles requires a two-temperature ($T_e \neq T_p$) collisional treatment (see Somov 1992). For what follows, it is important that the chromospheric plasma heated by accelerated particles expands quickly into the corona, creating soft X-ray emission in closed magnetic loops. Such chromospheric "evaporation" driven by accelerated particle beams would be interesting to distinguish observationally from evaporation driven by thermal fluxes into the chromosphere.

Another important feature of soft X-ray emission is that the outer loops systematically have higher temperatures. This was observed, for example, in the cusp-shaped portion of the 1992 February 21 flare (Tsuneta et al. 1992). The temperature reaches the peak far outside the apparent bright soft X-ray loop. This is a "hot source" in the 1993 January 13 flare (Tsuneta 1996; Tsuneta et al. 1997). According to our model, these "high-temperature ridges" are presumably heated by thermal conductive fluxes directly from the high-temperature current sheet (Oreshina & Somov 1996).

Further development required for our model is a quantitative consideration of the upward motion of the coronal hard and soft X-ray sources predicted by the model. It is clear that superhot plasma heated and compressed inside the collapsing trap will unavoidably relax in the downstream flow behind the shock. This relaxation is strongly influenced by thermal conductive cooling as well as by radiative energy losses, and finally by the chromospheric evaporation and thermal instability mentioned in § 2.3. The dynamics of superhot plasma relaxation may not be simple and will depend on initial and boundary conditions.

The behavior of the magnetic field behind the shock seems to be more strictly determined; the incoming field lines simply accumulate between the magnetic obstacle and the shock front. Hence, the shock front must move upward together with the hard X-ray source on the upstream side (Fig. 5) and the soft X-ray source on the downstream side. This prediction of the model has to be considered quantitatively and compared with apparent motion of coronal X-ray sources observed with the HXT and SXT on board *Yohkoh*.

5.5. *Behind-the-Limb Flares*

In principle, the hard X-ray observations could show nonthermal processes (acceleration, trapping, shock-associated phenomena) in the corona as clearly as do the radio observations. A behind-the-limb flare is the best case for such studies. However, a few observations have suggested a truly coronal origin for hard X-ray emission; the following conclusions have been drawn from these observations.

First, the coronal hard X-ray emission may lie above even the high loops responsible for soft X-ray production (Hudson 1978). Our model just explains the existence of such a hard X-ray above-the-loop-top source.

Second, the simple thick-target precipitation model does not explain the intensities of hard X-ray emission observed at different altitudes in the corona. Moreover, the introduction of an electron trap by magnetic mirrors could be useful, if the mirroring points were located high in the corona (Kosugi 1987). According to our model, the fast shock wave above the soft X-ray loop reflects particles back into the collapsing magnetic trap.

Third, coronal hard X-ray bursts have smoother time profiles in comparison with the chromospheric footpoint hard X-ray spikes (Hudson 1978; Wang et al. 1995). We think that the time profile of hard X-ray emission of accelerated electrons inside the trap can be described in terms of its

"effective capacitance," similar to the time dependence of an electric current inside an electric circuit. The ability to store electric charge makes variations of the electric current smoother; in just the same way, the larger the ability of the trap to accumulate accelerated electrons, the smoother the time profile of their emission in hard X-rays.

Fourth, coronal hard X-ray bursts may have relatively hard spectra (Hudson 1978; Kosugi, Dennis, & Kai 1988). We have not computed the energy spectrum of accelerated electrons inside the collapsing trap, but we are faced with the natural conclusion that the lower energy electrons are less confined in the trap. In addition to this obvious fact, we have seen in § 5.2 that the efficiency of the electron acceleration by the collapsing trap rapidly grows with increase of the initial energy $\mathscr{E}_{in}$ of the electrons preaccelerated by the HTTCS. Therefore, the resulting spectrum of electrons inside the trap should be rather hard. MeV electrons can be responsible not only for hard X-ray emission but also for microwaves in the so-called extended flares (Kosugi et al. 1988).

We believe that the collapsing trap model gives us a qualitative understanding of all known properties of hard X-ray emission in the flares placed behind the solar limb.

6. DISCUSSION

6.1. *Collisionless Reconnection*

The collisionless transformation of the magnetic energy into kinetic energy of particles inside a nonsteady two-dimensional reconnecting current sheet was introduced by Syrovatskii (1966) as a dynamic dissipation. An essential peculiarity of the dynamic dissipation is that the inductive strong electric field (see § 2.1) is directed along the current inside the reconnecting current sheet. Hence the field does positive work on charged particles, thus increasing their energy rapidly.

Naturally, some instabilities may be excited in the plasma-beam system inside the current sheet. Wave-particle interactions can transform a part of this work into direct heating of ions and electrons. Thus the collisionless driven reconnection leads to energy conversion from the field to the particles through acceleration and heating processes (e.g., Drake & Kleva 1991).

Three-component collisionless driven reconnection (e.g., Ono et al. 1996; Horiuchi & Sato 1997; Cai & Lee 1997) includes several natural complications that could be reviewed somewhere else. Particle simulation study of collisionless driven reconnection in a sheared magnetic field (Horiuchi & Sato 1997) shows that the electron acceleration and heating take place in the reconnection area. In the presence of a longitudinal magnetic field, the electron acceleration by the reconnection electric field is very efficient. Therefore, the general inference as to the possibility of particle acceleration and heating inside the collisionless RCS (i.e., dynamic dissipation of the magnetic field) remains valid and is used in the HTTCS model (Somov 1992). This allows us to consider the HTTCS as the primary source of flare energy and the first-step acceleration mechanism.

6.2. *Alternative Models*

In our model of a flare, the chromospheric evaporation driven by the beams of accelerated particles is the final stage in the chain of physical processes that includes the two-step acceleration of electrons and ions. In this sense, our model can be contrasted to the model by Bai et al. (1983). Our model also differs from that by Tsuneta (1995) for electron acceleration. The model by Tsuneta assumes the reconnection process as a primary mechanism of flare energy, as we do. However, the model does not consider the particle acceleration inside the reconnecting current sheet itself. Instead, it assumes that the fast downflow from the "reconnection site" collides with the loop, and that the resulting small-scale time-varying shear flows (vortices) at the loop top drive oppositely directed field-aligned currents (channels). The field-aligned currents then create voltage drops (≈ 100 keV) along the magnetic field lines, generating runaway electrons. Such a scenario seems to be consistent with "avalanche" models for flares (Lu & Hamilton 1991; LaRosa & Moore 1993) but has to be further developed to explain the properties of the above-the-loop-top source of hard X-ray emission.

LaRosa & Moore (1993) assume that fast plasma outflows from "sites of strongly driven reconnection" can generate the cascading MHD turbulence. Particles extract energy from this turbulence by mirroring on "magnetic compressions" moving along the magnetic field at the Alfvén speed. LaRosa et al. (1996), however, conclude that dissipation of the reconnection-generated MHD turbulence accounts for the electron bulk energization in solar flares but not the proton acceleration.

Acceleration of protons and heavier ions is an important advantage of our model. Since the first-order Fermi-type mechanism gives the energy gain that is proportional to the total energy of a particle, protons are accelerated more efficiently than electrons at the same velocity. Hence the solar flares with properties described by our models should produce energetic protons with a few-second delay related to the second-step acceleration of fast trapped protons by the shock wave. At the same time, the accelerated protons and ions, compared with the accelerated electrons, are much less frozen into the collapsing trap. Thus they have a larger probability of escaping from the trap to the open field lines directly into interplanetary space.

Acceleration of electrons to relativistic energies takes a time $\tau_a^{(e)}$ comparable to the time (eq. [19]) estimated for the 100 keV electrons. As a preliminary estimation of the time $\tau_a^{(e)} \approx$ a few seconds, we can use the consideration of the similar problem by Bai et al. (1983) in relativistic approximation. However, a more accurate consideration of the trapping and acceleration efficiency in the frame of our model is necessary.

7. CONCLUSION

We suggest a new model for a two-step acceleration of electrons and ions to high energies in solar flares. The first step is the very efficient acceleration of particles by the strong electric field inside a collisionless reconnecting current sheet—the primary source of flare energy. Being in a high-temperature state, the current sheet produces two very fast flows of collisionless "superhot" plasma. The downward flow of superhot plasma collides with a magnetic "obstacle" and creates the fast oblique collisionless shock similar to the terrestrial bow shock between solar wind and the Earth magnetosphere.

Reconnected field lines rapidly move out of the high-temperature turbulent-current sheet, being frozen into superhot plasma, and form magnetic loops on the upstream side of the shock front. Hence, the electrons and ions ener-

gized and preaccelerated by the current sheet appear to be trapped inside magnetic loops. The top of each loop moves with a high speed toward the shock, while both of its feet penetrate through the shock front. We argue that the "collapse" of the trap by the convection of the magnetic field lines through the shock should be accompanied by a considerable increase of particle energies. This seems to be similar to the so-called shock spike events observed near fast-mode interplanetary shock waves.

We therefore assume that the second-step mechanism is a very efficient combination of the fast "adiabatic heating" inside the collapsing trap and drift acceleration by the shock at the two feet of the trap. The lifetime of an individual collapsing loop can be identified with the observed few-second delay in higher energies of hard X-ray and gamma-ray emission.

Our model explains spatial distributions and behavior of X-ray emission in solar flares observed by the HXT and SXT on board *Yohkoh*. Trapped accelerated electrons can be seen as a thin-target hard X-ray source located above the soft X-ray–emitting loops. The altitude of this "above-the-loop-top source" must grow in time because reconnected field lines are continuously accumulated on the downstream side of the shock between the magnetic "obstacle" and the shock front. Precipitation of the accelerated electrons gives the thick-target hard X-ray emission in the footpoint sources and also generates the chromospheric evaporation driven partially by the electron beam and partially by anomalous heat-conductive fluxes of flare energy.

One of the authors (B. V. S.) would like to thank the National Astronomical Observatory of Japan for financial support. We are grateful to our colleagues L. Acton, T. Bastian, H. Hudson, S. Masuda, T. Sakao, K. Shibasaki, K. Shibata, T. Terasawa, S. Tsuneta, and Y. Uchida for stimulating and useful discussions. We wish to thank the referee for evaluating this paper and for helping us to clarify several arguments.

REFERENCES

Aschwanden, M. J., Bynum, R. M., Kosugi, T., Hudson, H. S., & Schwartz, R. A. 1996a, ApJ, submitted
Aschwanden, M. J., Hudson, H., Kosugi, T., & Schwartz, R. A. 1996b, ApJ, 464, 985
Aschwanden, M. J., Kosugi, T., Hudson, H. S., Wills, M. J., & Schwartz, R. A. 1996c, ApJ, 470, 1198
Aschwanden, M. J., Wills, M. J., Hudson, H. S., Kosugi, T., & Schwartz, R. A. 1996d, ApJ, 468, 398
Bai, T., Hudson, H. S., Pelling, R. M., Lin, R. P., Schwartz, R. A., & von Rosenvinge, T. T. 1983, ApJ, 267, 433
Balogh, A., & Erdos, G. 1991, J. Geophys. Res., 96(A9), 15853
Blandford, R. D. 1994, ApJS, 90, 515
Cai, H. J., & Lee, L. C. 1997, Phys. Plasmas, 4, 509
Dennis, B. R. 1988, Sol. Phys., 118, 49
Diakonov, S. V., & Somov, B. V. 1988, Sol. Phys., 116, 119
Drake, J. F., & Kleva, R. G. 1991, Phys. Rev. Lett., 66, 1458
Erdos, G., & Balogh, A. 1994, ApJS, 90, 553
Feldman, U., Hiei, E., Phillips, K. J. H., Brown, C. M., & Lang, J. 1994, ApJ, 421, 843
Fermi, E. 1954, ApJ, 119, 1
Field, G. B. 1965, ApJ, 142, 531
Giovanelli, R. G. 1946, Nature, 158, 81
Gisler, G., & Lemons, D. 1990, J. Geophys. Res., 95(A9), 14925
Gopalswamy, N., Raulin, J.-P., Kundu, M. R., Nitta, N., Lemen, J. R., Herrmann, R., Zarro, D., & Kosugi, T. 1995, ApJ, 455, 715
Gurevich, A. V., & Zhivlyuk, Yu. N. 1966, Soviet Phys.—JETP, 22, 153
Hesse, M., Birn, J., Baker, D. N., & Slavin, J. A. 1996, J. Geophys. Res., 101(A5), 10805
Hones, E. W., Jr., ed. 1984, Magnetic Reconnection in Space and Laboratory Plasmas (Washington, DC: AGU)
Horiuchi, R., & Sato, T. 1997, Phys. Plasmas, 4, 277
Hudson, H. S. 1978, ApJ, 224, 240
Jones, F. C., & Ellison, D. C. 1991, Space Sci. Rev., 58, 259
Kosugi, T. 1987, Sol. Phys., 113, 295
———. 1996, in AIP Conf. Proc. 374, High Energy Solar Physics, ed. R. Ramaty, N. Mandzhavidze, & X.-M. Hua (New York: AIP), 267
Kosugi, T., Dennis, B. R., & Kai, K. 1988, ApJ, 324, 1118
Kosugi, T., et al. 1991, Sol. Phys., 136, 17
LaRosa, T. N., & Moore, R. L. 1993, ApJ, 418, 912
LaRosa, T. N., Moore, R. L., Miller, J. A., & Shore, S. N. 1996, ApJ, 467, 464
Lin, R. P., & Hudson, H. S. 1976, Sol. Phys., 50, 961
Litvinenko, Yu. E., & Somov, B. V. 1991, Soviet Astron. Lett., 17, 353
———. 1993, Sol. Phys., 146, 127
———. 1995, Sol. Phys., 158, 317
Longcope, D. W., & Cowley, S. C. 1996, Phys. Plasmas, 3, 2885
Lu, E. T., & Hamilton, R. J. 1991, ApJ, 380, L89
Masuda, S., Kosugi, T., Hara, H., Sakao, T., Shibata, K., & Tsuneta, S. 1995, PASJ, 47, 677
Masuda, S., Kosugi, T., Hara, H., Tsuneta, S., & Ogawara, Y. 1994, Nature, 371, 495
Ono, Y., Yamada,M., Akao, T., Tajima, T., & Matsumoto, R. 1996, Phys. Rev. Lett., 76, 3328
Oreshina, A. V., & Somov, B. V. 1996, Astron. Rep., 40, 263
Sakao, T., & Kosugi, T. 1996, in Magnetodynamic Phenomena in the Solar Atmosphere: Prototypes of Stellar Magnetic Activity, ed. Y. Uchida, T. Kosugi, & H. S. Hudson (Dordrecht: Kluwer), 169
Somov, B. V. 1992, Physical Processes in Solar Flares (Dordrecht: Kluwer)
———. 1994, Fundamentals of Cosmic Electrodynamics (Dordrecht: Kluwer)
Somov, B. V., & Spektor, A. R. 1982, Space Sci. Rev., 32, 27
Speiser, T. W. 1965, J. Geophys. Res., 70, 4219
Sweet, P. A. 1969, ARA&A, 7, 149
Syrovatskii, S. I. 1966, Soviet Astron.—AJ, 10, 270
———. 1981, ARA&A, 19, 163
Takakura, T., Inda, M., Makishima, K., Kosugi, T., Sakao, T., Masuda, S., Sakurai, T., & Ogawara, Y. 1993, PASJ, 45, 737
Tanaka, K. 1987, PASJ, 39, 1
Thomas, V. A., & Winske, D. 1990, J. Geophys. Res., 95(A11), 18809
Toptyghin, I. N. 1980, Space Sci. Rev., 26, 157
Tsuneta, S. 1995, PASJ, 47, 691
———. 1996, ApJ, 456, 840
Tsuneta, S., et al. 1991, Sol. Phys., 136, 37
Tsuneta, S., Hara, H., Shimizu, T., Acton, L. W., Strong, K. T., Hudson, H. S., & Ogawara, Y. 1992, PASJ, 44, L63
Tsuneta, S., Masuda, S., Kosugi, T., & Sato, J. 1997, ApJ, in press
Wang, H., Gary, D. E., Zirin, H., Kosugi, T., Schwartz, R. A., & Linford, G. 1995, ApJ, 444, L115
Wang, J., Shibata, K., Nitta, N., Slater, G. L., Savy, S. K., & Ogawara, Y. 1997, ApJ, in press
Wentzel, D. G. 1963, ApJ, 137, 135
Wheatland, M. S., & Melrose, D. B. 1995, Sol. Phys., 185, 283